Journal of Geology and Mining Research

volume 6 Number 2 March, 2014

ISSN 2006-9782

Academic Journals

ABOUT JGMR

The **Journal of Geology and Mining Research (JGMR)** (ISSN: 2006-9766) is an open access journal that provides rapid publication (monthly) of articles in all areas of the subject such as mapping of deformed rock bodies, recovery of natural resources, geotechnical engineering, numerical modelling in geological studies etc.The Journal welcomes the submission of manuscripts that meet the general criteria of significance and scientific excellence. Papers will be published shortly after acceptance. All articles published in JGMR are peer-reviewed.

The **Journal of Geology and Mining Research** (ISSN: 2006-9766) is published twice a month (one volume per year) by Academic Journals.

Contact Us

Editorial Office: jgmr@academicjournals.org

Help Desk: helpdesk@academicjournals.org

Website: http://www.academicjournals.org/journal/JGMR

Submit manuscript online http://ms.academicjournals.me/

Editors

Prof. D.P. Tripathy
Head, Department of Mining Engineering National Institute of Technology, Rourkela-769008. India.

Prof. K.C. Tiwari
Department of Geology The Maharaja Sayajirao University of Baroda VADODARA - 390 002 Gujarat State – India

Dr. D.S Subrahmanyam
Geotechnical Engineering Division, National Institute of Rock Mechanics,(Govt. of India) ITI Annex Building, Dooravani Nagar Bangalore, Karnataka – 560 016

Journal of Geology and Mining Research

Table of Content: Volume 6 Number 2 March 2014

ARTICLES

Research Articles

academicJournals

Vol. 6(2), pp. 18-27, March, 2014
DOI: 10.5897/JGMR14. 0197
Article Number: ADF262F46969
ISSN 2006 – 9766

http://www.academicjournals.org/JGMR

Journal of Geology and Mining Research

Review

Mafic and ultramafic rocks in parts of the Bhavani complex, Tamil Nadu, Southern India: Geochemistry constraints

Ali Mohammed Dar[1]*, Akhtar R. Mir[2], K. Anbarasu[1], M. Satyanarayanan[3], V. Balaram[3], D. V. Subba Rao[3] and S. N. Charan[3]

[1]Department of Geology, Periyar University, Salem, Tamilnadu-636011, India.
[2]Department of Earth Science, University of Kashmir, Srinagar-190006, India.
[3]National Geophysical Research Institute, Council of Scientific and Industrial Research, Uppal Road, Hyderabad-500606, India.

Received 9 January, 2014; Accepted 19 February, 2014

Present paper deals with the petrogenesis of gabbros and pyroxenites of Bhavani complex, Tamil Nadu, Southern India. Studied gabbros are mainly composed of pyroxenes with minor plagioclase (An_{10-30}) and amphibole minerals. Pyroxenites are composed of coarse-grained clinopyroxenes, orthopyroxenes and medium-grained hornblende minerals. Geochemically, in the total alkali vs. SiO_2 diagram studied samples are broadly classified as gabbros and their magma type is tholeiitic in nature, however, based on the TiO_2, MnO, P_2O_5 diagram most of the studied samples fall within the calc-alkaline basaltic (CAB) field. In chondrite-normalized rare earth element (REEs) patterns, pyroxenites show negative Eu anomaly with slight enrichment of heavy rare earth elements (HREEs). The negative Eu anomaly in these samples indicates fractionation of plagioclase. The flat chondrite-normalized REEs pattern of gabbros in association with low CaO, Al_2O_3, Sr content and absence of Eu anomaly suggest removal of plagioclase component from basic parental magma. In primitive mantle (PM) and mid-ocean ridge basalt (MORB) normalized incompatible trace element patterns studied samples have enrichment of large ion lithophile elements (LILEs) and light rare earth elements (LREEs). Tectonic setting discrimination diagrams, in addition to their geochemical characteristics such as Nb-Ta, Zr-Hf negative anomalies and low values of (La/Yb)cn and (La/Sm)cn, suggest volcanic arc tectonic setting.

Key words: Bhavani, layered complex, Geochemistry, light rare earth elements (LREEs), large ion lithophile elements (LILEs), petrogenesis.

INTRODUCTION

The Bhavani ultramafic complex and Sittampundi ultrabasic complex is considered to be age of 2898 ± 50 Ma years arrived at by the Sm-Nd systematics (Bhaskara Rao et al., 1996). According to Bhaskar Rao et al. (1996)

*Corresponding author. E-mail: mtekali@gmail.com

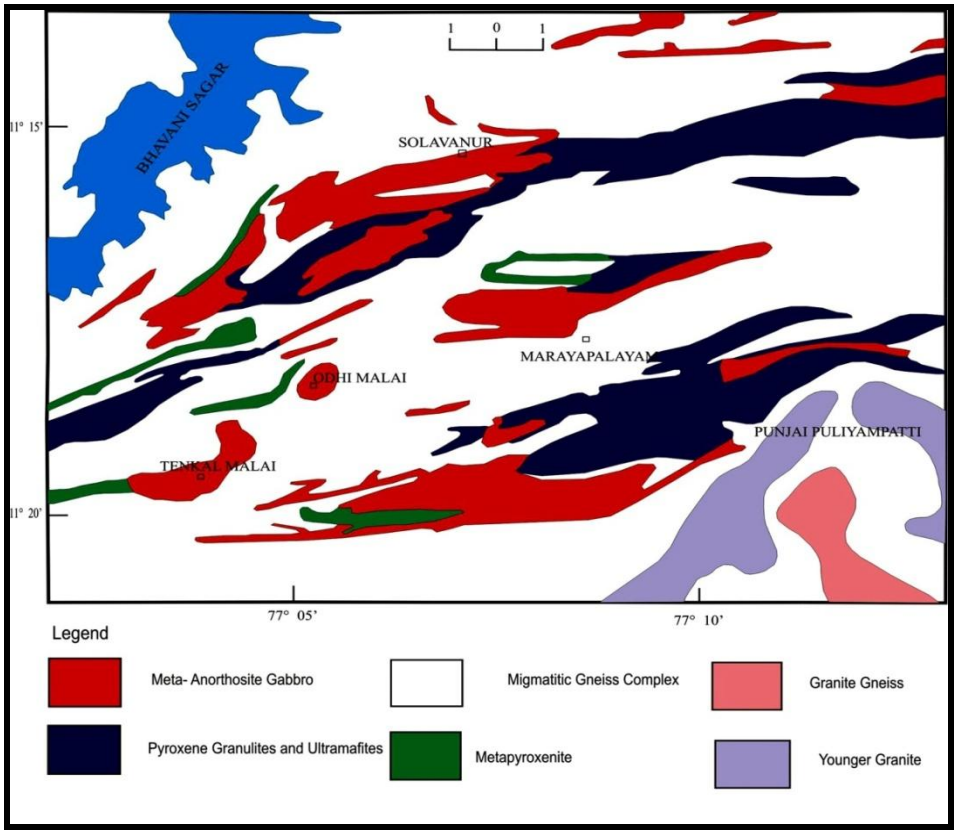

Figure 1. Geological map of Bhavani complex showing distribution of E-W trending mafic-ultramafic rocks after Selvan (1981).

the rocks of Bhavani layered complex, was subjected to three phases of deformation. The earliest of these was in the form of tight isoclinal folds with an E-W axis, followed by the second phase of coaxial tight synformal and antiformal folds. These two deformation phases led to the interleaving of the components of the Bhavani Layered Complex with those of Sathyamangalam Group. During the course of the third phase of deformation, there was cross-folding and slicing up of the complex, giving rise to structural domes and basins. Due to intense deformation and mineral segregation, the gabbroic rocks exhibit banded structures with alternating leucocratic and melanocratic bands. A group of ultrabasic rocks ranging in composition from dunite, peridotite, garnetiferous gabbro, gabbroic anorthosite to anorthosite are traced along the Bhavani river valley in the Coimbatore and the Erode districts of Tamil Nadu, South India, forming part of the Bhavani Layered Complex (Selvan, 1981; Subramanian and Selvan, 2001). These bodies are considered to be emplaced in the weak zones of deep-seated fractures in crustal rocks and emplaced into the rocks of the Sathyamangalam Group. There is a dearth of petrological and geochemical data on mafic and ultramafic rocks of the Bhavani Layered Complex. The present paper embodies the results of the petrological and geochemical analysis of mafic and ultramafic rocks of Odhimalai and Thenkalmalai areas located within the Bhavani Complex (Figure 1). Odhimalai is a bi-symmetrical hillock with an altitude of 654 m above Mean Sea Level (MSL) and elevated about 250 m from the base of the hill. The Thenkalmalai is a linear ridge with an altitude of ~ 389 m above MSL. Both of the hillocks are striking ENE – WSW directions.

GEOLOGIC SETTING

In Palghat–Cauvery suture zone, dismembered units of Archaean layered complexes comprising calcic-meta anorthosites, websterites, clinopyroxenite, pyroxenite, mafic granulites and serpentinised dunite occur as linear bands for a distance of more than 250 km. from the southern margin of Nilgiri massif to Sittampundi in the east. The detailed field studies of two hillocks (Odhimalai and Thenkalmalai) lead to the recognition of an array of rock types including metagabbro, meta-anorthositic gabbros, pyroxenites, and peridotite, occurring as layers in close association (Rao et al., 1996). The dominant member of both the hillocks is metagabbro and pyroxenite / metapyroxenite. They show a flat E-W

Table 1. A stratigraphic sequence for Bhavani complex.

Age (Ma)	Group	Major rock type	Era
390 -550	Younger granite	Granite	Proterozoic to Palaeozoic
700 - 900	Ultrabasics / basics younger	Gabbro, Anorthosite	
1600 - 2100	Basic intrusives	Gabbro/Dolerite dyke	Meso Proterozoic
2600	Charnokite group	Charnokite Pyroxene granulite	Late Archaean
3000 - 3100	Mettupalayam complex	Meta-anorthosite Meta-gabbro Meta-pyroxenite Dunite	Archaean
3200	Sathyamangalam group	Amphibolite, basic/ ultrabasic rocks Sillimanite-kyanite-corundum-mica schist Fuchsite-kyanite ferruginous quartzite	Archaean
	Basement	Basement Gneiss	

trending linear bodies showing sub-parallelism to the trend of main shear. The ultramafic and mafic association in the study area shows a dissected pattern and occurs as enclaves within the Peninsular gneisses. Macroscopically, the meta-gabbros are characterized by color indices ranging from approximately 65 to 95 m, with the mafic minerals being dominated by pyroxene, amphibole, and garnet (Rao et al., 1996). Plagioclase feldspar is the dominant light colored mineral in these rocks. Magnetite and ilmenite can also be readily identified in hand sample. The mafic bands meanwhile have an average width of only a couple of millimeters. The weathering makes surface outcrops slightly bumpy, whereas the hand samples tend to be much darker, especially on freshly cut surfaces. The second most litho unit in the present study area is pyroxenite/meta pyroxenite. In Odhimalai, the pyroxenite occurs all along its eastern margin and displays layered contact with metagabbro. In Thenkalmalai the pyroxenite occupies almost half of the hill lock and shears equal proportion whereas in Odhimalai the gabbro is dominant over the pyroxenite. In hand specimen the pyroxenite shows greenish black color along the fringes of outcrop and towards core it becomes darker. Comparing grain size of pyroxenites at both locations are medium to coarse grained. The medium-grained pyroxenites form the important litho unit in the Odhimalai hillock where as the coarse- grained pyroxenites are mostly observed in the Thenkalmalai hillock. In Thenkalmalai area pyroxenite and gabbro shears equal proportion where as in Odhimalai the gabbro is dominant over the pyroxenite (Figure 1). The third most abundant rock type observed in the field area is a meta-anorthositic gabbro, however this lithology is mostly confined to Odhimalai area only and ranges in thickness from 0.5 to 5 m towards the top of hillock. The rocks overall show a granoblastic polygonal microtexture and display disequilibrium textures (like symplectitic coronas) mostly in metagabbroic rocks containing garnet (Rao et al., 1996). A stratigraphic sequence for the Bhavani complex modified form geological survey of India miscellaneous publication No. 30 is given in Table 1.

PETROGRAPHY

Petrographic description was performed on 20 thin sections. In hand specimen, the gabbros are dark brownish in colour, whereas the pyroxenites are dark grayish in colour. In thin section gabbros are relatively plagioclase poor (average plagioclase abundances of 10 to 25%) and pyroxene rich. Orthopyroxene is typically coarse grained and is characterized by subhedral crystal surface provided indication of magmatic origin. The plagioclase is mainly equigranular; medium grained and display polygonal texture with angular crystal margins. The plagioclase grains show polysynthetic twinning on albite law. Most of the grains show strain effect in the form of wavy extinction.

Pyroxenites in thin section are texturally characterized by distinct adcumulate texture. They are quite mafic and probably represent pyroxene rich and plagioclase poor portion of cumulate. These pyroxenites are composed of coarse-grained clinopyroxenes, orthopyroxenes and medium grained hornblende crystals. Most of the grains show euhedral crystal surfaces. The accessory phase being the magnetite and ilmenite, concentrated characteristically along the grain boundaries. Clinopyroxenes occur as equigranular coarse euhedral to subhedral grain associated with few interstitial opaques. A few of them exhibit two microtextural features such as exsolution texture and the Fe-Ti oxide rod lets along the

cleavage planes. The coarse grains of clinopyroxenes in pyroxenites display exsolution texture defined by very thin orthopyroxenes with parallel extinction. They are regularly spaced and uniformly distributed throughout the grain, reflecting a compositional gradient across the pyroxene during exsolution. These regularly spaced exsolution lamellae and uniform distribution support the mechanism of exsolution by a homogeneous nucleation and growth in a slowly cooling magmatic system (Buseck et al., 1980) rather than heterogeneous nucleation and growth in which irregular thicker pyroxene exsolution lamellae are developed.

GEOCHEMISTRY

Analytical methods

Whole-rock analysis

Total of sixteen representative samples, seven are pyroxenites and nine are gabbros, were analyzed for bulk chemistry at National Geophysical Research Institute (NGRI) Hyderabad, India. Major elements were determined by X-ray fluorescence Spectrometry (XRF) using Philips MAGIX PRO Model 2440. Trace elements were analyzed by Inductive Coupled Plasma mass Spectroscopy (ICP-MS) using a Perkin Elmer SCIEX ELAN DRC II. The procedure, precision and detection limits are the same as given by Balaram and Rao (2003).

Major, trace, and rare earth element (REEs) data of pyroxenites and gabbros of the Bhavani Complex, Tamil Nadu are given in Table 2. The geochemical signatures of the gabbros and pyroxenites show a significant variation in major and trace elements. The SiO_2 abundance covers a narrow compositional range in the pyroxenites (49.6-55.5 wt. %) and gabbros (50.1-58 wt. %). The gabbros are characterized by low TiO_2 (0.26-0.54 wt. %). Whereas the pyroxenites show slighty high concentration of TiO_2 (0.24-1.7 wt. %). MgO content varies from (7.4-13.1 wt. %) in gabbros and (3.6-14.3 wt. %) in pyroxenites. The pyroxenites show high concentration of total iron (8.4-16 wt. %), MgO (3.6-14.3 wt. %) with moderate enrichment of TiO_2 (0.24-1.7 wt. %) and depleted alkalies Na_2O (0.39-2.5 wt. %); K_2O (0.03-1.5 wt. %). The CaO-Al_2O_3 relationship of both pyroxenite and gabbro show their trend towards primordial mantle with Al_2O_3/CaO ratio of >1 in majority of samples (Figure 2). The studied samples have CaO/Al_2O_3 ratios ranging from (0.78-1.8) which is higher as compared to the primordial mantle CaO/Al_2O_3 ratio (0.79) (Hoffmann, 1988). Relative to primordial mantle, the pyroxenites and gabbros show the enriched trend in SiO_2, TiO_2, Total iron, CaO, Na_2O, and depleted trend in MgO (Table 2). In the alkali-SiO_2 diagram (Figure 3) almost all the samples are broadly classified as gabbro. Bulk composition/whole rock analyses indicate that the magma type is tholeiitic but trending towards a calc-alkaline nature; this inference is also supported by AFM diagram (after Irvine and Baragar, 1975) (Figure 4). A plot for SiO_2-K_2O (Figure 5) after Peccerillo and Taylor, 1976) indicates that the samples belong to low-K tholeiitic series. Jensen (1976) cation plot uses Al_2O_3, $FeO^{(t)}$ + TiO_2 and MgO cations because of the stability of these elements during metamorphism. The plot (Figure 6) indicates that most of the samples cluster on the border of high-Fe (HFT) and high-Mg (HMT) tholeiitic basalt. Some of the samples are Mg-rich and plot in the basaltic komatiitic (BK) field. The plot again indicates that there is an overall tholeiitic affinity of the magma trending towards a calc-alkaline nature. Based on the TiO_2, MnO, P_2O_5 diagram (proposed by Mullen, 1983) most of the studied samples fall within the Calc-alkaline basaltic (CAB) field (Figure 7). Thus it could be inferred that the tectonic environment of eruption is volcanic arc environment and the studied samples fall within the Calc-alkaline basaltic field. Concentration of compatible trace elements in pyroxenites like V (273-309 ppm), Cr (9877-13342 ppm), Co (87-111 ppm) and Ni (676-1055 ppm) are high while these pyroxenites are poor in incompatible and HFS elements like Rb, Hf, Ta, Th, and U. Sr shows a remarkable low concentration ranging from (0.37-0.94 ppm). Similar pattern are observed in gabbro samples being enriched in compatible trace elements and poor in incompatible and HFS elements. Total REE value of pyroxenites varies from 10.13-13.99 ppm with limited REE, (Ce_N/Yb_N = 0.55-0.69) and LREE fractionation (La_N/Sm_N = 1.32-1.66). The HREE also conclude limited fractionation (Gd_N/Yb_N = 0.49-0.58) with negative Eu anomaly. The total REE values of gabbros varies from (12.01-23.48 ppm) with limited REE fractionation (Ce_N/Yb_N = 0.62-1.77). LREE (La_N/Sm_N = 0.54-1.68) and HREE fractionation is also within limited range (Gd_N/Yb_N = 1.19-1.37) with negligible Eu anomaly.

Chondritie-normalized REE plot of the pyroxenites reflects negative Eu anomaly with slight enrichment of HREE (Figure 8). The negative Eu anomaly in these samples may be interpreted as due to fractionation of plagioclase ± hornblende and can be imposed when the melt phase enters the stability field of plagioclase. The Low LREE and slight enriched trend of HREE may be due to retention of these elements somewhat by clinopyroxenes or to a greater extent by hornblende. The chondritie-normalized REE plot of gabbros show a flat REE pattern with gentle or without any Eu anomaly (Figure 9). The flat REE pattern in association with low CaO, Al_2O_3, Sr content and absence of Eu anomaly suggests removal of plagioclase component from basic parent magma or may be due to the magma that might have segregated at such depth where plagioclase is not stable and hence it could not be fractionated (Barker et al., 1976). The representative PM and MORB normalized trace element plots for the pyroxenites and gabbros are presented in (Figure 10 and 11a, b). Relative to PM and

Table 2. Representative major (wt %) and trace (ppm) element composition of gabbros and pyroxenites from Thenkalmalai and Odhimalai (Mettupailium Ultramafic complex), Tamilnadu, Southern India.

Rock type	Gabbro								Pyroxenite								PM*
Sample No	OM-06	OM-07	OM-08	OM-13	OM-22	OM-23	OM-25	OM-33	OM-48	OM-32	OM-37	OM-38	OM-39	OM-40	OM-45	OM-52	
SiO_2	51.5	52.3	50.1	51.5	58	53.5	54	54	49.9	55.5	51.8	52.6	51.4	51.8	49.6	53.9	45.96
TiO_2	0.36	0.41	0.35	0.37	0.32	0.3	0.26	0.39	0.54	0.88	0.65	0.24	1.7	0.42	0.58	0.45	0.18
Al_2O_3	11.0	12.8	9.4	9.7	9.9	12.4	11.5	12	13	13.1	13.6	8.4	10.6	13.7	13	6	4.06
Fe_2O_3	10.4	10.7	16.9	16.2	11.2	11.4	15	10.3	13.9	13.5	16	8.4	15.4	11.8	12.6	15.8	7.54
MnO	0.16	0.15	0.25	0.16	0.12	0.13	0.12	0.13	0.18	0.19	0.21	0.11	0.19	0.17	0.13	0.23	0
MgO	11.9	10.0	13.1	10.2	11.1	11.3	7.4	12.1	9	3.6	6.5	14.3	6.6	8	10.3	7.9	37.78
CaO	13.4	12.2	9	10.6	8.7	10.4	11.2	10.4	12.1	10.9	8.4	15.5	12.6	12.7	10.3	15.1	3.21
Na_2O	1.1	1.3	0.76	1	0.41	0.41	0.41	0.55	1.3	1.9	2.5	0.39	1.2	1.2	1.7	0.53	0.33
K_2O	0.08	0.11	0.10	0.20	0.08	0.07	0.08	0.11	0.06	0.32	0.13	0.05	0.24	0.09	1.5	0.03	0
P_2O_5	0.02	0.03	0.02	0.03	0.01	0.02	0.01	0.01	0.03	0.07	0.08	0.01	0.06	0.03	0.24	0.02	0
Total	**9.92**	**100**	**99.98**	**99.96**	**9.84**	**99.93**	**99.98**	**100**	**99.96**	**99.87**	**100**	**99.99**	**99.91**	**99.95**	**99.96**	**99.06**	**99.99**
Sc (ppm)	44.9	43.2	45.7	47.3	45.6	52.5	46.5	47.3	46.8	9.9	8.9	8.6	7.7	8.5	8	7.9	
V	195.2	205.5	219.3	235.3	304.1	180.2	222.3	260.5	242.7	298.6	286.5	288.3	263	307.7	309.4	273.7	
Cr	957.6	1683.2	1240.3	1188.4	82.6	2291.9	12007.5	546.1	778.9	21200.4	10690.4	12720.9	13342.2	11503	11938	9877.1	
Co	44.6	75.7	53	54.3	49.6	57.3	53.2	55.8	49.5	111.5	102.5	108.7	104.4	106.1	94.1	87.1	
Ni	188.6	249.4	196.7	186	81.6	305	192	151.7	163.3	1055.4	894.5	1016.5	990.5	851.3	676.8	1013.4	
Cu	35.3	33.9	23.7	26.9	21.4	19.1	39.9	34.5	30.2	60.7	66.3	59	115.7	34.8	90.2	78	
Zn	42.8	51.0	38.7	50.4	45.9	52.3	66.7	51.7	53	72.3	57.4	73.8	83	59.4	64.2	46.6	
Rb	1.7	2.5	3.5	1.4	1.4	1.6	1.5	1.5	2.8	16.4	9.7	4.4	6	4.3	11.2	5.5	
Sr	6.3	4.8	4.6	5.2	4.9	1.4	4.6	4.1	2	0.57	0.71	0.44	0.53	0.37	0.39	0.94	
Y	0.33	0.30	0.36	0.42	0.53	0.27	0.40	0.50	0.5	1.9	2.2	2.1	1.7	2.2	2.4	2.1	
Zr	0.12	0.11	0.17	0.16	0.11	0.16	0.15	0.15	0.16	0.27	0.32	0.27	0.24	0.37	0.3	0.28	
Nb	0.25	0.42	0.31	0.28	0.75	0.22	0.35	0.25	0.34	3.7	4.4	4.3	4.3	4.7	4.8	4.8	
Ba	18.7	6.7	4.9	3.9	7.7	4.0	4.4	3.1	5.2	19.6	6.6	8	5.8	6.8	7	8.2	
Hf	0.18	0.14	0.22	0.21	0.23	0.18	0.22	0.22	0.24	0.42	0.43	0.45	0.36	0.55	0.49	0.46	
Ta	0.04	0.07	0.04	0.04	0.10	0.03	0.05	0.03	0.04	0.01	0.04	0.05	0.08	0.02	0.02	0.15	
Th	0.17	0.22	0.07	0.07	0.07	0.09	0.09	0.07	0.13	1.3	1.2	1.5	1.03	1.2	0.72	2.7	
U	0.09	0.07	0.05	0.0	0.12	0.19	0.15	0.11	0.18	0.13	0.05	0.21	0.1	0.08	0.1	0.25	
La	2.53	1.63	1.48	1.35	2.50	1.37	1.26	0.93	1.21	1.16	1.02	1.28	0.83	1.30	1.05	1.15	
Ce	4.46	3.88	3.74	3.34	5.62	2.83	3.17	2.33	2.92	2.93	2.91	2.94	2.26	3.40	3.08	2.88	
Pr	0.56	0.56	0.53	0.48	0.82	0.42	0.54	0.42	0.47	0.34	0.34	0.37	0.28	0.38	0.39	0.36	
Nd	3.01	3.23	2.89	2.85	4.95	2.50	3.34	2.86	3.14	1.71	1.91	1.83	1.46	1.94	2.08	1.82	
Sm	0.94	0.89	0.86	0.92	1.49	0.74	1.06	1.06	1.08	0.44	0.48	0.45	0.38	0.50	0.52	0.45	

Table 2. Contd

Eu	0.37	0.30	0.33	0.38	0.59	0.26	0.36	0.41	0.37	0.12	0.13	0.12	0.11	0.14	0.14	0.12
Gd	1.18	1.01	1.03	1.28	1.75	0.87	1.21	1.40	1.46	0.79	0.85	0.89	0.67	0.89	0.95	0.89
Tb	0.20	0.16	0.19	0.23	0.29	0.16	0.21	0.27	0.27	0.16	0.17	0.18	0.14	0.20	0.20	0.18
Dy	1.54	1.24	1.45	1.80	2.20	1.18	1.66	2.12	2.01	1.38	1.48	1.49	1.18	1.55	1.71	1.49
Ho	0.35	0.27	0.32	0.39	0.50	0.26	0.36	0.48	0.47	0.35	0.38	0.37	0.31	0.39	0.44	0.38
Er	0.98	0.79	0.90	1.10	1.32	0.71	1.01	1.31	1.29	1.12	1.26	1.21	1.02	1.28	1.43	1.26
Tm	0.13	0.10	0.12	0.14	0.17	0.09	0.13	0.17	0.16	0.18	0.21	0.19	0.17	0.20	0.23	0.20
Yb	0.76	0.59	0.71	0.81	1.05	0.51	0.76	1.01	0.98	1.20	1.42	1.26	1.13	1.33	1.51	1.31
Lu	0.16	0.13	0.16	0.18	0.23	0.11	0.17	0.22	0.22	0.21	0.25	0.24	0.20	0.25	0.26	0.23
Pb	6.08	5.9	6.10	4.20	5.17	4.71	5.19	5.29	5.96	0.01	0.02	0.01	0.02	0.01	0.01	0.01
∑REEs	17.17	14.78	14.71	12.25	23.48	12.01	15.24	14.99	16.05	12.08	12.81	12.83	10.13	13.75	13.99	12.73
Ce_N/Yb_N	1.58	1.77	1.42	1.11	1.44	1.49	1.13	0.62	0..80	0..66	0.55	0.63	0.54	0.69	0.55	0.59
La_N/Sm_N	1.68	1.14	1.07	0.91	1.04	1.15	0.74	0.54	0.70	1.66	1.32	1.76	1.35	1.62	1.25	1.58
Gd_N/Yb_N	1.28	1.41	1.19	1.30	1.37	1.41	1.31	1.14	1.23	0.54	0.49	0.58	0.49	0.55	0.52	0.56
Eu/Eu*	1.06	0.96	1.06	1.06	1.11	.98	0.96	1.02	0.89	0.62	0.61	0.57	0.65	0.63	0.60	0.57
Rb/Nb	7.51	6.69	12.69	5.76	2.14	8.03	4.71	6.65	9.31	4.97	2.48	1.14	1.54	1.03	2.64	1.27
Th/Nb	5.71	4.38	1.90	2.10	0.78	3.41	2.16	2.34	3.18	2.95	2.24	2.91	1.98	2.15	1.26	4.67

PM* = Primordial mantle major oxides data after Hofmann (1988). $Fe_2O_3^t$ = Total iron as Fe_2O_3.

MORB, both set of rocks show enrichment of LILEs and LREEs. They are further characterized by a low Th abundance and a distinct Nb-Ta, Zr-Hf troughs.

These features are characteristic of tholeiitic basalts produced at destructive plate margins or within plate tholeiites which are contaminated by continental crust (Hawkesworth et al., 1994). The depletion of Nb is not affected by the fractional crystallization and it is known that Nb anomaly in modern arc volcanic is independent of the degree of crystallization.

Since the Nb is not transferable into slab, the depletion of Nb is thought to reflect formation in supra-subduction zone tectonic setting (Brique and Joron, 1984).

PETROGENSIS

The whole-rock chemical data can provide useful information on the course of fractional crystallization/magmatic evolution. The various binary diagrams (Figure 12) have been plotted in order to evaluate the evolution of the studied samples. The MgO has been taken as the reference value because of its wide range and plays an important role in process of fractional crystallization. The studied samples show increasing trend of SiO_2, K_2O+ Na_2O, Fe_2O_3 and TiO_2 with the decrease of MgO whereas CaO and CaO/Al_2O_3show decreasing trend with the decrease of MgO. A positive correlation observed between CaO, CaO/Al_2O_3 and MgO supports the fractionation of clinopyroxenes. During the plagioclase removal, CaO/Al_2O_3 ratio increases whereas it remains constant during olivine fractionation (Dungan and Rnodes, 1978). Thus it could be inferred that the high value of CaO/Al_2O_3 ratio (greater than 0.8) in the studied samplesmay be due to plagioclase fractionation. Fractional crystallization associated with crustal contamination is an important process during magmatic evolution (De-Paolo, 1981) and may modify both elemental and isotopiccompositions. Crustal materials are rich in LILEs, K_2O and Na_2O and depleted in P_2O_5 and TiO_2. Low concentration and narrow range of K_2O and Na_2O in the investigated samples suggests in favor of their minimal crustal contamination.

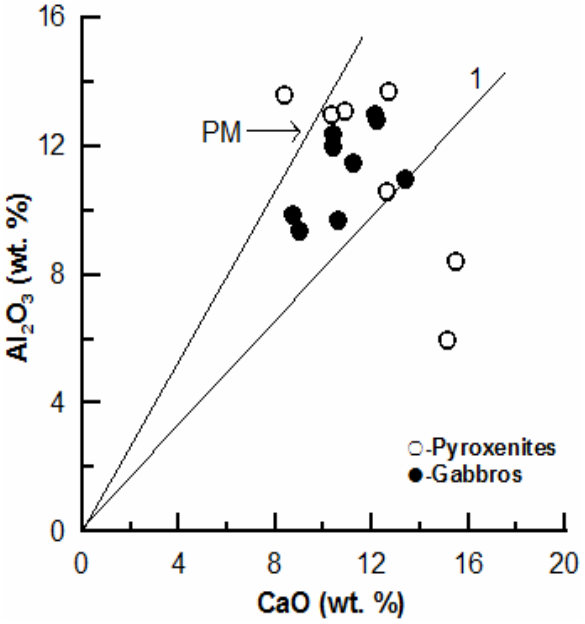

Figure 2. CaO vs Al_2O_3 diagram depicts that the CaO content of gabbros and pyroxenites tends to be close to primordial mantle array (Hoffman, 1988).

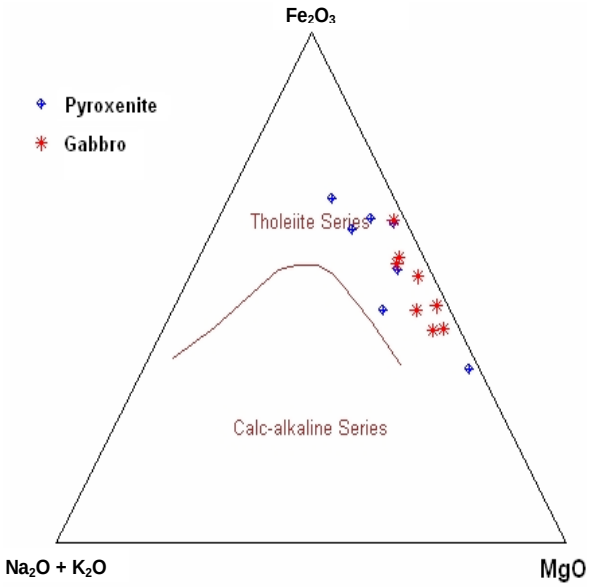

Figure 4. AFM diagram for gabbros and pyroxenites (after Irvine and Baragar, 1975).

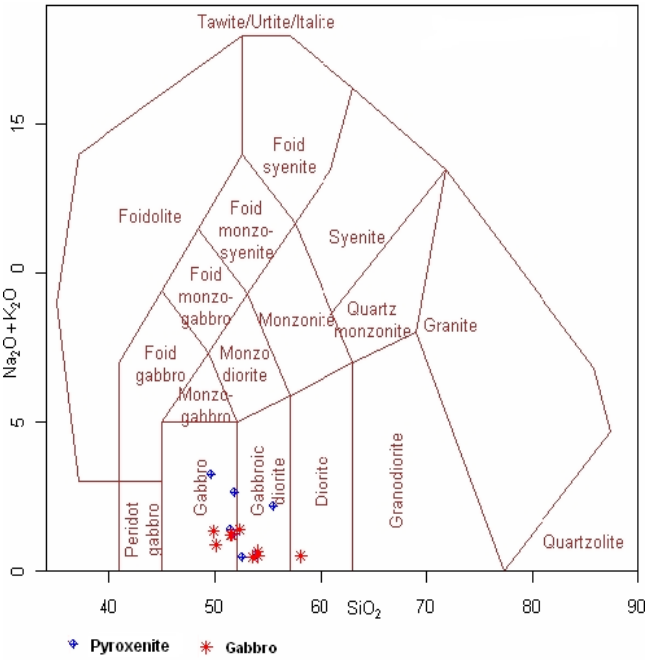

Figure 3. Rock classification diagram (Total alkali Vs SiO_2) after Middlemost (1985).

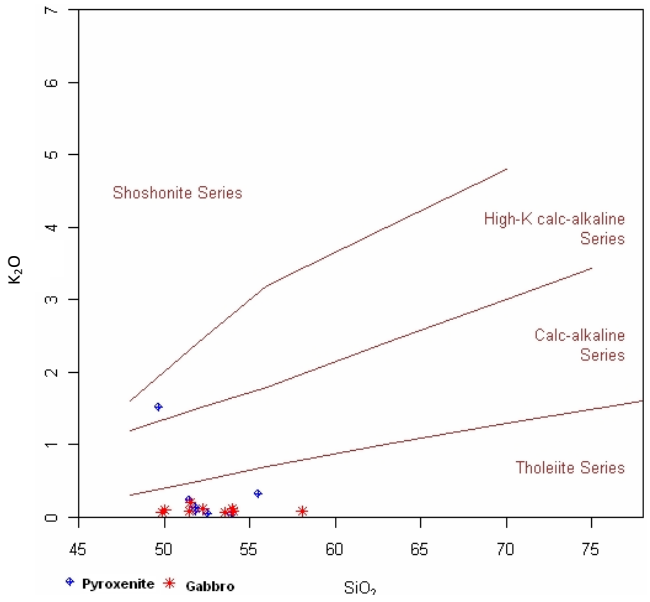

Figure 5. Rock classification diagram (K_2O vs SiO_2 after Peccerill and Taylor 1976).

The values of Nb/La and Nb/Ce of the studied samples show that the gabbros have a quite low range of Nb/La and Nb/Ce (0.09-0.3) and (0.05- 0.13), where as the pyroxenites show slightly high range of Nb/La (3.18-5.24) and Nb/Ce (1.25-1.92) respectively. These values for gabbros are not only very low compared to those of primitive mantle (PM 1.02 and 0.40, respectively, Taylor and McLennan, 1985; 1.04 and .40, respectively, Sun and McDonough, 1989) but are also lower than the average bulk crust (0.69 and 0.33 respectively). Such lower values are not expected to be produced by processes of contamination by an average crustal

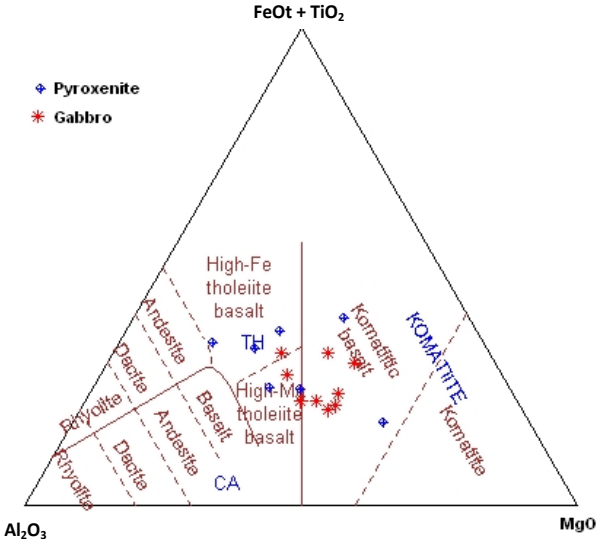

Figure 6. Jensen's cation Plot for gabbros and pyroxenites (after Jensen 1976).

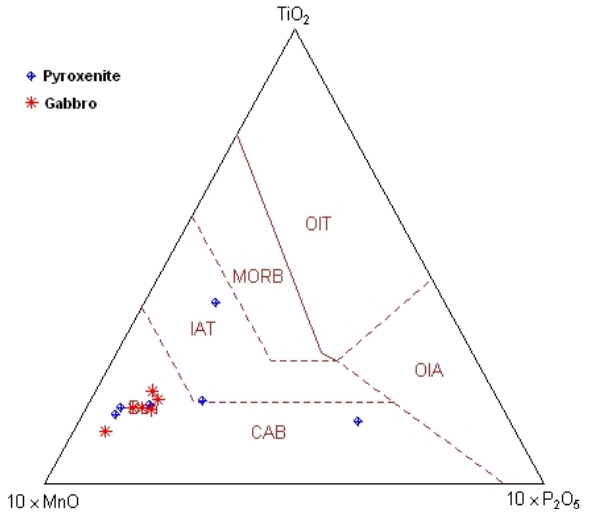

Figure 7. TiO_2-MnO-P_2O_5 triplot for gabbros and pyroxenites (after Mullen 1983).

component. Thus, it can be inferred that these trace element characteristics may have been obtained by studied rocks due to LREEs-LILEs enriched source characteristics with depletion of high field strength elements (such as Nb) at plate margin settings (Weaver and Tarney, 1983; Ahmad and Tarney, 1994; Mir et al., 2011, 2013). Enrichment of LILEs and depletion of HFSEs may also occur in within plate tectonic setting rocks due to crustal contamination, but, studied rocks show least crustal contamination.The geochemistry of mafic and ultramafic rocks is most commonly used to discriminate tectonic setting.

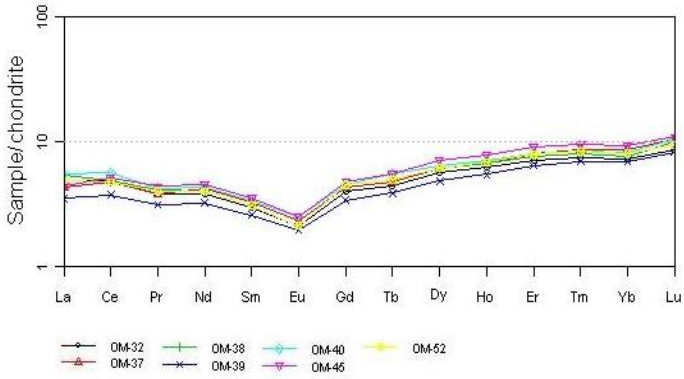

Figure 8. Chondrite normalized REE diagram for the pyroxenites after Sun and McDonough (1989).

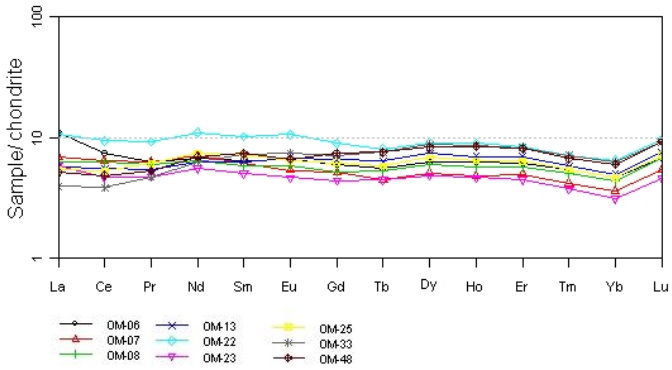

Figure 9. Chondrite normalized REEs diagram for the gabbros from Bhavani ultramafic complex normalized after Sun and McDonough (1989).

According to Pearce and Cann (1973) it is possible to use geochemistry to distinguish between basalts produced in different known tectonic settings. The basaltic rocks are formed in almost every tectonic environment and they are believed to be geochemically sensitive to the changes in plate tectonic frame work. In order to understand the tectonic environment of the studied samples the plot Ti/1000 vs. V (after Shervais, 1982) shown in Figure 13 depicts that the studied samples fall in the Arc tholeiitic environment. To support this, tri-plot proposed by Mullen (1983). Figure 6 shows that the majority of the samples fall in the calcic-alkaline basaltic field of arc environment. In addition, geochemical ratios such as La/Yb and La/Sm are good indicators of mantle sources and degree of melting (Verma, 2006; Mir et al., 2011). Rift rocks show high (La/Yb)cn and (La/Sm)cn values, where as arc/ back arc show low values of both parameters (Verma, 2006). Therefore the low values of both parameters (La/Yb)cn <2.31 and (La/Sm)cn <1.76 in the studied samples may indicate the volcanic arc setting.

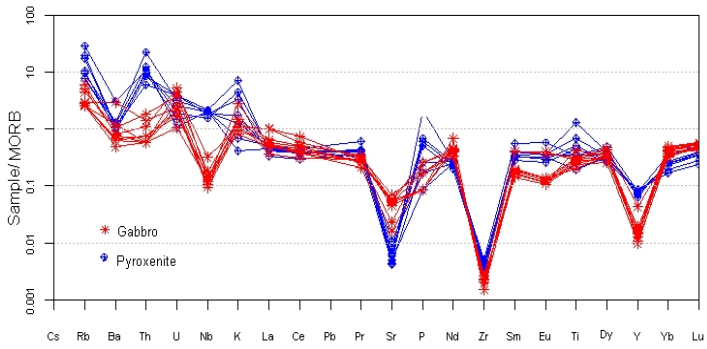

Figure 10. MORB normalized diagram for gabbros and pyroxenites after Sun and McDonough (1989).

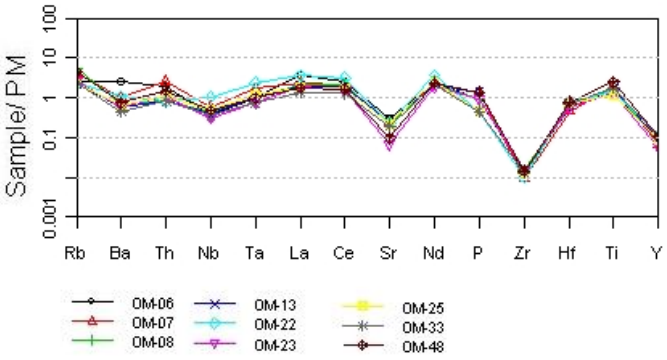

Figure 11b. Primitive element-normalizes multi-element diagram for gabbros after Sun and McDonough (1989).

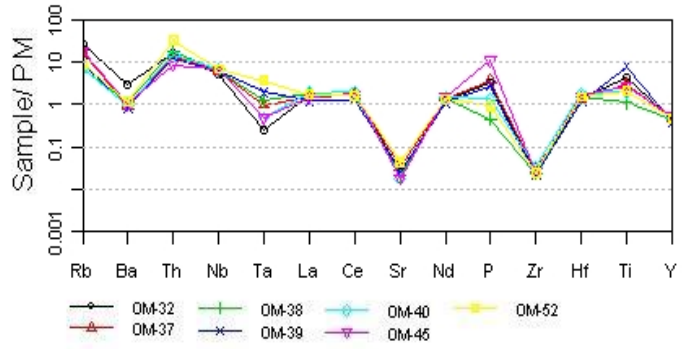

Figure 11a. Primitive element-normalizes multi-element diagram for pyroxenites after Sun and McDonough (1989).

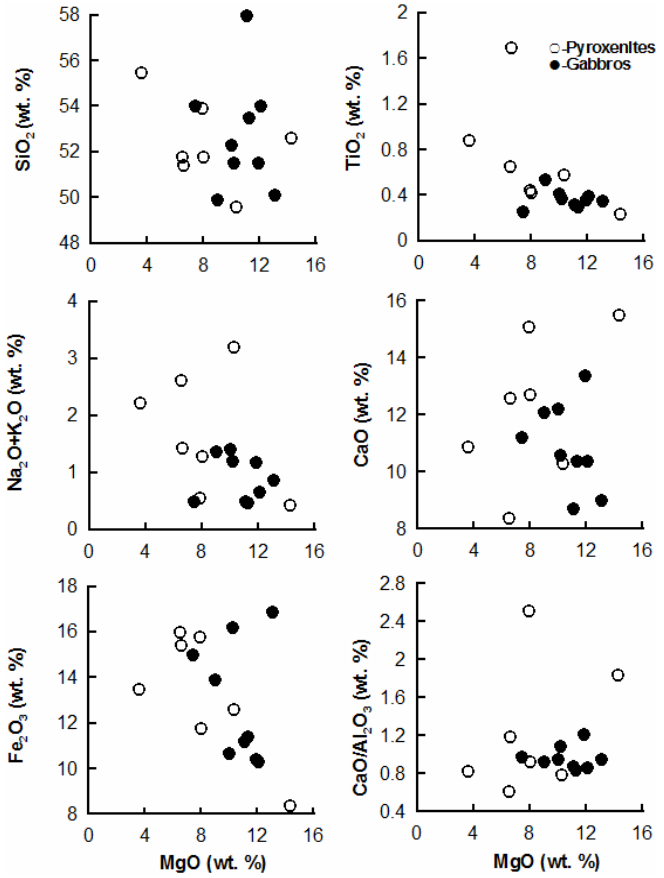

Figure 12. Binary plots of gabbros and pyroxenites: MgO Vs, SiO_2, : MgO Vs Na_2O+K_2O, : MgO Vs Fe_2O_3, : MgO Vs TiO_2, : MgO Vs CaO , : MgO Vs CaO/Al_2O_3.

CONCLUSIONS

On the alkali-SiO_2 diagram almost all the studied samples are broadly classified as gabbros. On the bases of relationship among major oxides such as SiO_2, K_2O, Al_2O_3, FeO(t), TiO_2 and MgO magma type of studied samples is tholeiitic in nature, however, based on the TiO_2, MnO, P_2O_5 diagram most of the studied samples fall within the calc-alkaline basaltic (CAB) field. Thus it could be inferred that the tectonic environment of eruption is volcanic arc environment. Low concentration and narrow range of K_2O and Na_2O in the investigated samples suggests in favor of their least crustal contamination. Low values of Nb/La and Nb/Ce in studied gabbros also discourages the crustal contamination. The negative Eu anomaly in pyroxenites depicts fractionation of plagioclase. The Low LREEs and slight enriched trend of HREEs may be due to retention of these elements somewhat by clinopyroxenes or to a greater extent by hornblende. The condritic normalized REEs plot of gabbros show a flat REEs pattern with gentle or without any Eu anomaly**.** The flat REEs pattern in association with low CaO, Al_2O_3, Sr content and absence of Eu anomaly suggests removal of plagioclase component from basic parent magma. In addition to tectonic setting discrimination diagrams their geochemical characteristics

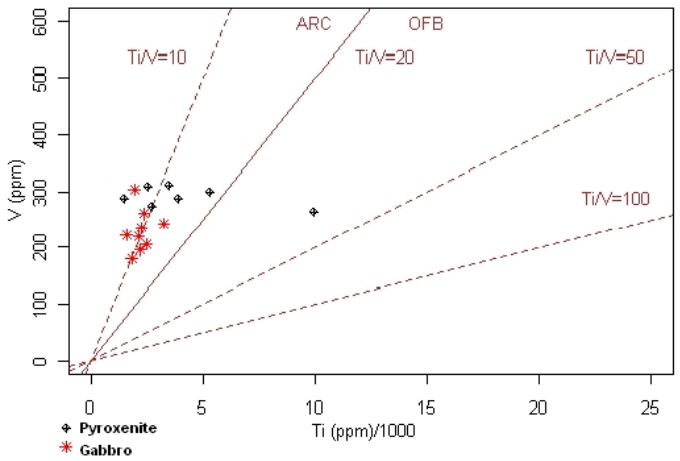

Figure 13. Ti/1000 Vs V tectonic discrimination diagram (after Shervais 1982) for gabbros and pyroxenites.

such as low Th abundance, significant Nb-Ta and Zr-Hf anomalies, low values of (La/Yb)cn and (La/Sm)cn favours the inference of arc tectonic setting of these rocks.

Conflict of Interests

The author(s) have not declared any conflict of interests.

REFERENCES

Ahmad T, Tarney J (1994). Geochemistry and petrogenesis of late Archean Aravalli olcanic, basement enclaves and granitoids, Rajasthan. Precamb. Res. 65:1-23. http://dx.doi.org/10.1016/0301-9268(94)90097-3

Balaram V, Rao TG (2003). Rapid determination of REE and other trace elements in geological samples by microwave acid digestion and ICP-MS. Atom. Spectrosc. 24:206-212.

Barker F, Arth JG, Peterman ZE, Friedman I (1976). The 1.7 to 1.8-b.y. old trondhiemites of south western Colorado and northern new mexico. Geochemistry and depth of genesis. Geol. Soc. Am. Bull. 87:189-189. http://dx.doi.org/10.1130/0016-7606(1976)87<189:TTBTOS>2.0.CO;2

Bhaskar Rao YJ, Chetty TRK, Janardhan AS, Gopalan K (1996). Sm–Nd andRb-Sr ages and P–T history of the Archean Sittampundi and Bhavani layeredmeta-anorthosite complexes in Cauvery shear zone, South India: evidence forNeoproterozoic reworking of Archean crust. Contrib. Mineral. Petrol. 125: 237–250. http://dx.doi.org/10.1007/s004100050219

Brique L, Bougault Joron JL (1984). Quantification of Nb, Ta, Ti, and V anomalies in magamas associated with Subduction zones: petrogenitic implication. Earth Planet. Sci. Lett. 68:297-308. http://dx.doi.org/10.1016/0012-821X(84)90161-4

De-Paolo DJ (1981). Trace element and isotopic effects of combined wallrock assimilation and fractional crystallization. Earth Planet. Sci. Lett. 53:189-202. http://dx.doi.org/10.1016/0012-821X(81)90153-9

Dungan MA, Rnodes JM (1978). Residual glasses and melt inclusions in basalts from DSDP Legs 45 and 46: evidence for magma mixing. Contrib. Mineral. Petrol. 67:417-431. http://dx.doi.org/10.1007/BF00383301

Hawkesworth CJ, Gallagher AK, Hergt JM, Mcdermott BF (1994). Destructive plate margin magmatism: Geochemistry and melt generation. Lithos 33:169-188. http://dx.doi.org/10.1016/0024-4937(94)90059-0

Hoffmann AW (1988). Chemical differentiation of the earth: the relationship between mantle, continental crust and oceanic crust. Earth planet. Sci. Lett. 90:297-314. http://dx.doi.org/10.1016/0012-821X(88)90132-X

Irvine TA, Baragar WRA (1975). A guide to the chemical classification of the common volcanic rocks. Canad. J. Earth Sci. 8:523-546. http://dx.doi.org/10.1139/e71-055

Jensen LS (1976). A new cation plot for classifying subalkalic volcanic rocks. Min. Nat. Resources Ontario Division of Mines Misc paper 66:20.

Middlemost EAK (1985). Naming materials in the magma/igneous rock system. Earth-Sciences Reviews 37:215-224. http://dx.doi.org/10.1016/0012-8252(94)90029-9

Mir AR, Alvi SH, Balaram V (2011). Geochemistry of the mafic dykes in parts of the Singhbhum Granitoid complex: petrogenesis and tectonic setting. Arab. J. Geos. 4:933-943. http://dx.doi.org/10.1007/s12517-010-0121-6

Mir AR, Alvi SH, Balaram V, Bhat FA, Sumira Z, Dar SA (2013). A subduction zone geochemical characteristic of the newer dolerite dykes in the singhbhum craton, Eastern India. Inter. Res. J. Geol. Min. 3:213-223.

Mullen ED (1983). MnO/TiO2/P2O5: a minor element discriminant for basaltic rocks of oceanic environments and its implications for petrogenesis. Earth Planet. Sci. Lett. 62:53-62. http://dx.doi.org/10.1016/0012-821X(83)90070-5

Pearce JA, Cann JR (1973). Tectonic setting of basic volcanic rocks determined using trace element analyses. Earth Planet. Sci. Lett. 19:290-300. http://dx.doi.org/10.1016/0012-821X(73)90129-5

Peccerillo A, Taylor SR (1976). Geochemistry of Eocene calc-alkaline volcanic rocks from the Kastamonu area, Northern Turkey. Contrib. Mineral. Petrol. 58:63-81. http://dx.doi.org/10.1007/BF00384745

Rao YJB, Chetty TRK, Janardhan AS, Gopalan K (1996). Sm-Nd and Rb-Sr ages and P-T history of the Archean Sittampundi and Bhavani layered meta-anorthosite complexes in Cauvery shear zone, South India: evidence for Neoproterozoic reworking of Archaean crust. Contrib. Mineral. Petrol. 125: 237-250. http://dx.doi.org/10.1007/s004100050219

Selvan TA (1981) Anorthosite-gabbro-ultramafic complex around Gobichettypalayam, Tamil Nadu and their possible relation to Sittampundi type anorthosite complex (unpublished). Ph.D. thesis Univ Mysore Mysore India.

Shervais JW (1982). Ti-V Plots and Petrogenesis of modern and ophiolitic Lavas. Earth Planet. Sci. Lett. 59: 108–118. http://dx.doi.org/10.1016/0012-821X(82)90120-0

Sun S, McDonough WF (1989). Chemical and isotopic systematic of oceanic basalts: implications for mantle composition and processes. In: Saunders AD, Norry MJ (Eds), Magmatism in the ocean basins. Geol. Soc. London Sp. Pub. 42:313-345.

Subramanian KS, Selvan TA (2001). Geology of Tamil Nadu and Pondicherry. Geol. Soc. India (Text-book series). P. 192.

Taylor SR, Mclennan SM (1985). The continental crust: its composition and evolution. Blackwell, Oxford.

Verma SP (2006). Extension-related origin of magmas from a garnetbearing source in the Los Tuxtlas volcanic field, Mexico. Int. J. Earth Sci. (Geol Rundsch) 95:871-901. http://dx.doi.org/10.1007/s00531-006-0072-z

Weaver BL, Tarney J (1983). Chemistry of the sub continental mantle inferences from Archean and Proterozoic dykes and continental flood basalts. In: Hawkesworth CJ, Norry MJ (eds) Continental Basalt and Mental Xenoliths. Shiva Nantwich: pp. 209-229.

academicJournals

Vol. 6(2), pp. 28-38, March, 2014
DOI: 10.5897/JGMR14. 0200
Article Number: C2F1F7846973
ISSN 2006 – 9766

http://www.academicjournals.org/JGMR

Journal of Geology and Mining Research

Full Length Research Paper

Recent uranium mobilization and radioactivity of metamorphosed sandstones at Sikait area, South Eastern desert of Egypt

Soliman A. Abu Elatta[1], S. F. Hassan[1], A. H. El-Farrash[2], M. G. El-Feky[1]* and M. Refaat[1]

[1]Nuclear Material Authority, El-maadi, Cairo, Egypt.
[2]Physics Department, Faculty of Science, Mansoura University, Mansoura, Egypt.

Received 24 February, 2014; Accepted 25 March, 2014

The metamorphosed sandstones exposures occur in two locations in Wadi Sikait. The exposed rocks in this area are ophiolitic mélange, metamorphosed sandstones, porphrytic granites invaded by post-granite dykes (lamprophyres) and quartz-fluorite veins. The uranium contents measured radiometrically range from 3 to 41.97 ppm, with an average of 12 ppm, while the chemically measured are in the range from 20 to 100 ppm and averaging 50.83 ppm. High uranium contents are mainly attributed to the presence of secondary uranium minerals (uranophane and autonite), accessory minerals (monazite, zircon, allanite and xenotime) and U-bearing minerals (muscovite, biotite, chlorite, iron oxides and clays). P- and D-factors indicate disequilibrium in U-decay due to addition of uranium in these rocks. Since radioactive secular equilibrium of the young age deposits have not yet reached, therefore, the activity ratios (AR) of $^{230}Th/^{234}U$ in the studied rocks is very small and ranges from 0.43 to 1.3. Radon exhalation rates of the studied rocks were also measured using ''Sealed Can technique'' and indicated the presence of subsurface and surface uranium anomaly which confirms the previous results.

Key words: Metamorphosed sandstones, uranium, minerals, Wadi Sikait.

INTRODUCTION

The natural environmental radiation depends mainly on geological and geographical conditions (Florou and Kritidis, 1992). Higher radiation levels are associated with igneous rocks, such as granite and lower levels with sedimentary rocks. There are exceptions, however, as some shales and phosphate rocks have relatively high content of radionuclides (UNSCEAR, 1993). The study area lies in the southern part of the Eastern Desert of Egypt along the upper stream of Wadi Sikait (Figure 1).

Wadi Sikait area is covered by moderate to high mountains with rugged topography. The high peak is Gabal Sikait (769 m a.s.l); it is formed of ultramafic rocks, which are often associated with beryl mineralization. The Sikait area was geologically investigated by Hashad and El Redy (1979), Hegazy (1984), Hassan and Hashad (1990), Omar (1995), Mohamed and Hassanen (1997),

*Corresponding author. E-mail: mglal_99@hotmail.com

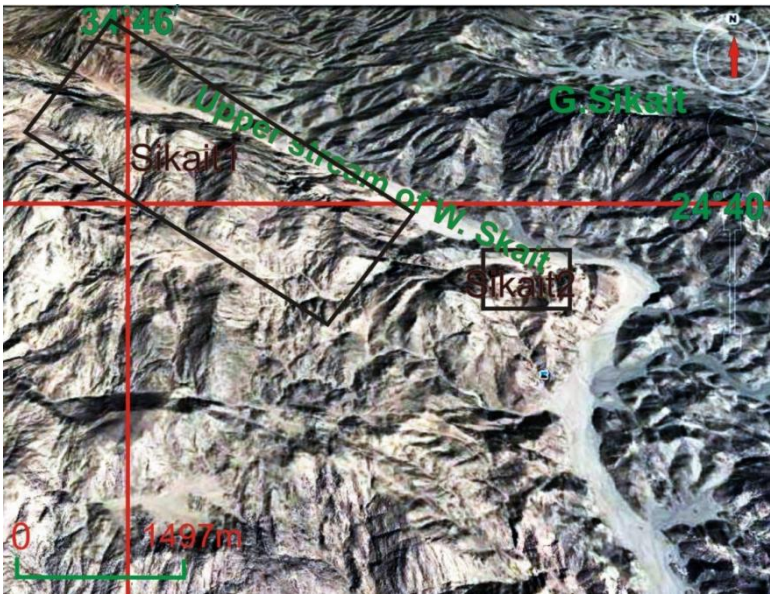

Figure 1. Aerial photograph showing Location of the studied areas.

Saleh (1998), Ibrahim et al. (1999) and Saleh et al. (2012), among others.

The Wadi Sikait area, in the south Eastern Desert of Egypt is located along the low-angle thrust zone of the Nugrus Thrust Fault (El-Ramly et al., 1984) and may represent a zone of discontinuity between two domains, the central and southern parts of the Eastern Desert (Stern and Hedge, 1985). This thrust fault separates the medium metamorphic grade associations, dominantly metapelites and gneiss, from the lower metamorphic grade ophiolitic melange assemblage, with subordinate metasediments in its footwall (Greiling et al., 1988; Harraz and EL-Sharkawy, 2001; Saleh et al., 2012). The region is composed of metapelitic schists, gneisses and granites and is cut by a number of dykes of different compositions, together with various types of aplitic and pegmatitic veins. Greiling et al. (1994) concluded that post collisional evolution in Eastern Desert of Egypt started with extensional collapse, which was followed by NNW-SSE shortening and related large - scale thrusting (toward the NNW) and folding, distributed all over the Eastern Desert, followed by further period of Late to Post-activity.

Assaf et al. (2000) studied the polyphase folding in Nugrus-Sikait area and reported that the lithological constitution of the area comprise a sequence of dismembered ophiolites, ophiolitic mélange association and arc assemblage. The older rocks are intensively deformed and intruded by intracratonic association, which, within the mapped area, is ophiolitic mélange, metamorphosed sandstones with porphyritic granites. Planer and linear mesoscopic structures exhibited by the rocks of the area indicate that these rocks are involved in superimposed folding events and at least three folding generations.

Detailed spectrometric radiometric study (Ibrahim et al., 2007) for metamorphosed sandstones site at Wadi Sikait indicate that eU range from (15 to 100 ppm), but chemically range from (60 to 480 ppm); whereas eTh was up to 85 ppm. Also, they reported that the emplacement of both lamprophyre dykes and porphyritic granites may play important role as a heat source, which lead to U-mobilization from hot granitic magma, transported (along deep fault and banding) and redeposited in metamorphosed sandstones under suitable conditions. The present work aims to study the radioactivity of Sikait metamorphosed sandstone and clarify the evidences of recent U-mineralization of these rocks.

METHODOLOGY

Analytical techniques

A variety of samples, comprising various degrees of alteration were investigated using the following five techniques: (1) Petrographic study, (2) autoradiographic analysis, (3) environmental scanning electron microscope examination, (4) NaI(Tl) and HPGe-detectors, and (5) uranium chemical analysis. An autoradiographic investigation was carried out for studying the forms of the radioactive mineralizations in the studied samples. Alpha-sensitive cellulose-nitrate film was sandwiched between the thin-polished section and a glass slide. Exposure time varied from 21 to 30 days. Calibration of NaI(Tl) detector was carried out by using Co-57 gamma source (122.1 KeV, set up in channel 122) and Cs-137 source (661.6 KeV, set up in channel 662). The unknown samples were measured through the system and then related to the standard sources of U, Th, Ra and K, provided by the International Atomic Energy Agency (IAEA). A computer program analysis,

written in Pascal language (Matoline, 1991) and run under MS-Dos, has been used to calculate the concentrations of (U, Th and Ra in ppm) and K (in %).

Geological setting

The field mapping indicates that metamorphosed sandstones occur in two sites at Wadi Sikait (Sikait-1 and Sikait-2) (Figure 1) and the exposed rocks at this area can be arranged based on field observations and structural relations from older to younger as follows:

1. Veins (fluorite and quartz) youngest;
2. Lamprophyre dykes;
3. Porphryitic granites;
4. Metamorphosed sandstones;
5. Ophioltic mélange oldest.

Ophiolitic mélange

The ophiolitic mélange in the study area occurs on the Eastern side of Wadi Sikait. It is composed of ophiolitic block rocks (mafic and ultramafic) tectonically embedded in highly pervasively deformed matrix of metasedimentary origin and rock fragments of meta-peridotite, meta-pyroxenite and meta-gabbros, different in sizes and shapes. The metasedimentary matrix is highly folded and sheared schists (quartzo-feldspathic schist, garnet micaschist, tourmaline-garnetiferous schist, graphite schist, sillimanite schist and talc schist). Also, many microstructures were found in the matrix as foliations, boudins, mineral lineations and minor folding. The most foliation planes are parallel to the plane of Nugrus thrust. The ophiolitic blocks represented about 2% of the total ophiolitic mélange and are characterized by highly serpentinized or transformed into talc-carbonate in many places with creamy color.

Metamorphosed sandstones

The metamorphosed sandstones occur in two locations in Wadi Sikait. The first location (Sikait-1) lies at the upper stream of Wadi Sikait and the second location (Sikait-2) occurs west the bend of Wadi Sikait (Figure 2a and b). The metamorphosed sandstone rocks are fine- to medium- grained, white color, highly sheared, sometimes beded, cross-cut by lamprophyre dykes (NW-SE and NNE-SSW), quartz veins and left strike slip faults (NW-SE, NNE-SSW and N-S) (Figure 3a). Sikait-1 is the largest outcrop of metamorphosed sandstones at Wadi Sikait, with low to medium peaks, elongated in NW-SE direction (1.4 km in length and range in width from 120 to 300 m) (Figure 3b). These rocks range in color from pale white to milky white (Figure 3c) and show relics of primary bedding; banding and obvious foliations in NW-SE with angle of dip 35°/SW (Figure 3d). Metamorphosed sandstones in this location are dissected by three types of left strike slip faults, N-S and NNE-SSW and NW-SE (Figure 3e), so that they are highly tectonized. The NW-SE is the largest and oldest one. These faults, especially NNE- SSW, are characterized by mylonitization and many types of alterations as silicification and Fe-Mn oxy-hydroxides (Figure 3f). Mineralization occurs along zones of these faults visible to the naked eyes.

Sikait-2 covers a small area where its length is about 450 m and maximum width about 230 m, forming low terrain, highly sheared, dissected by branches of strike slip fault running in N-S with left movements and frequently curved to N direction. Branch zones of the strike slip fault characterized silicification alteration. Many mineralizations are associated with quartz found along zones of fault branches as fluorite at west of this location and wolframite and cassiterite which are visible to naked eyes. Metamorphosed sandstones are generally uniform in texture and composed of fused quartz grains. Semi-angular and elongated rock fragments of older rocks are enclosed in metamorphosed sandstones.

Microscopically, the metamorphosed sandstones at this location are fine- to medium grained, with whitish grey color and vary in composition from greywacke to arkose. The secondary uranium minerals in these rocks at Sikait-1 are filling pore spaces between crystals, associated with the strike slip faults (especially NNE-SSW and NW-SE), or in both broken and surfaces of crystals near these faults (Figure 4a to d).

Greywacke is composed essentially of quartz, sodic plagioclase, K-feldspars and biotite as well as garnet and fluorite, zircon and allanite as accessories while chlorite and sericite (muscovite) is the alteration products. Quartz (66% in vol.) occur in two generations; the first one is euhedral shape, showing undulated extension and corroded in plagioclase while the second is squeezed among primary minerals and filling fractured plagioclase and may be formed related to the structured affected in the area. Plagioclase (An_{7-12}) is characterized by a representation of 32% in vol. of the rock, subhedral to anhedral crystals, highly deformed twinning and partially sericitized. K- Feldspars are represented by microcline, orthoclase and orthoclase microperthite phenocrysts. The longest axes of these crystals are parallel to the strike of foliation. K-Feldspars is subjected to the different degrees of kaolinitization. Biotite crystals occur as subhedral flakes and most of them showed foliations, partially altered to chlorite along their cleavages, showing foliations (Figure 4e). Sometimes biotite is distributed through the rock and/or sometimes segregated in folded layer. Muscovite occurs as aggregates associated with biotite or plagioclase. Zircon occurs as euhedral to subhedral prismatic crystals and some of them are metamict (Figure 4f). Allanite occurs as subhedral to anhedral crystals with among the same primary minerals. Fluorite occurs as considerable amount, filling the space among primary minerals or as inclusions in plagioclase. Garnet occurs as subhedral crystals.

Arkoses are composed essentially of quartz and feldspars as well as opaques, zircon and allanite while sericite is the main alteration product. Quartz (80% in vol.) occurs as polygonal shape and sometimes showed undulated extension as a result of the strain affected. Feldspars (18% in vol.) are represented by albite (14% in vol.) and perthite (4% in vol.). Albite occurs as subhedral to anhedral crystals, taking preferred orientation. Most of these crystals are cracked and corroded by/or contains quartz. Perthite crystals occur as anhedral cracked string type. Opaques are rare and occur as skeletal shape; zircon occurs as short prisms terminated by two pyramids. Allanite occurs as subhedral to anhedral crystals among the primary minerals.

Porphyritic biotite granite

Porphyritic biotite granite is characterized by grey to whitish pink color, coarse to very coarse-grained, with k-feldspars crystals up to 2 cm and composed mainly of quartz, plagioclase, k-feldspars and biotite. This rock is marked with sharp contacts with metamorphosed sandstones and contains xenoliths of it. Most k-feldspars crystals take preferred orientation parallel to the general direction of the biotite flakes. Porphyritic biotite granite cuts by both lamprophyre dykes and strike slip faults occur in study area. Strike slip faults are characterized by reddish color along fault zones, brecciate, gouge structure and barren quartz vein sometimes. Porphyritic biotite granite is mylonitized at the east side of the Sikait-2 due to affected major faults.

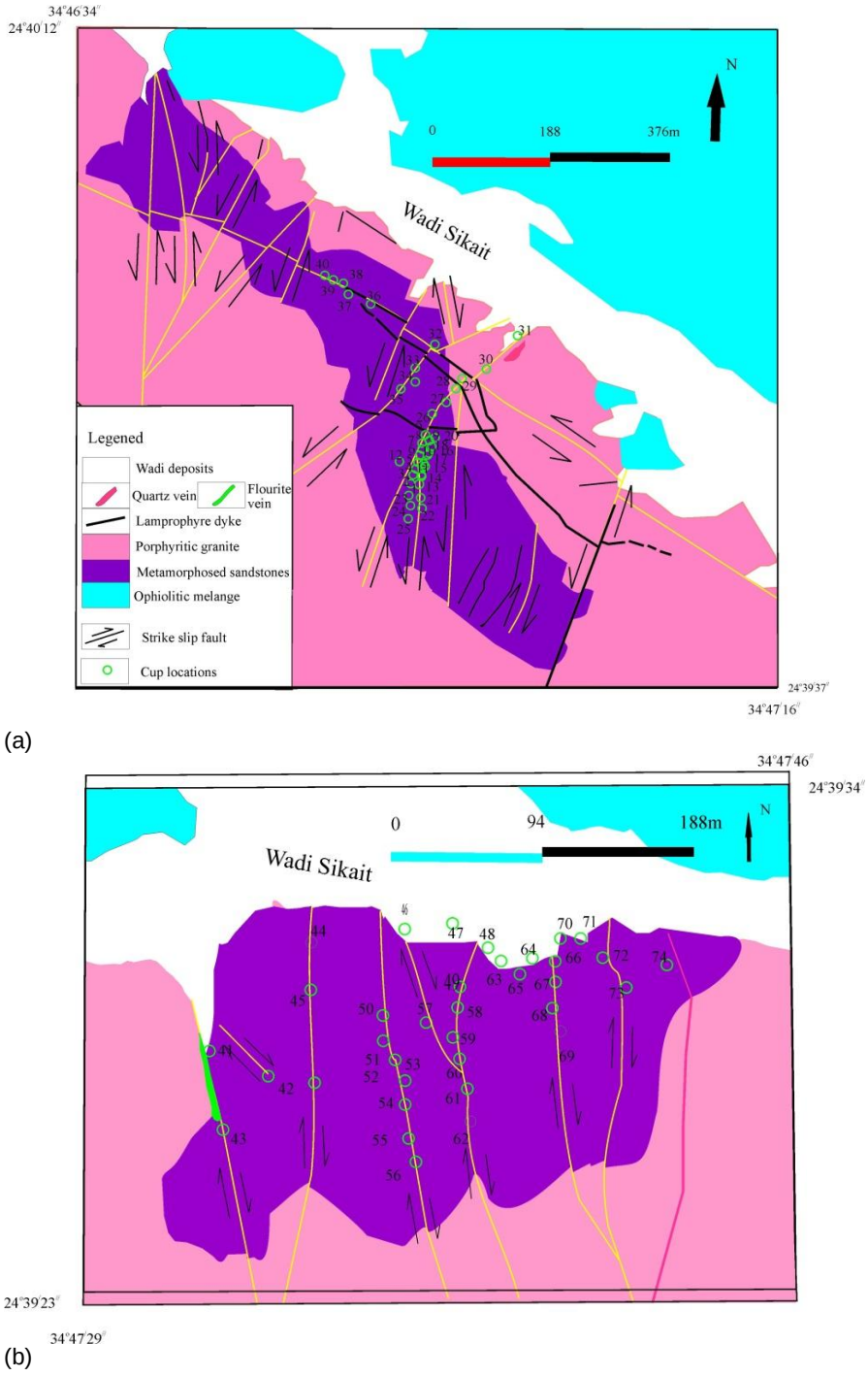

Figure 2. Detailed geologic map of Sikait-1(a) and Sikait-2 (b) (Ibrahim et al., 2010).

Lamprophyre dykes

Lamprophyre dykes are compact, black or dark black in color, altered, fine-grained, discontinuous and vary in thickness from 0.5 to 2 m and up to 1.4 km in length. These dykes cut both the metamorphosed sandstones and porphyritic biotite granite. The trends of these dykes are concordant with the main structural trends affected in the study area, so that they run in NW-SE, NNE-SSW and N-S.

Particle track analyses

Some samples from the different mineralized parts of metamorphosed sedimentary rocks were submitted to α-track analyses as a mean of micromapping the radioelement distribution.

Figure 3. Field photographs: (a) lamprophyre dyke runs NW-SE and cuts metamorphosed sandstone; (b) Lens-like of metamorphosed sandstone inliers within granitic rocks; (c) Alteration zone of metamorphosed sandstone; (d) relics of bedding in quartzite showing disturbed direction; (e) Left lateral movements of strike slip runs NNE-SSW; (f) hematitizations (Fe) and manganese oxides (Mn) along shear zones.

the rock with remarkable epidotization and sericitization of plagioclase. The biotite and muscovitc grains are enriched in uranium mineralization along their outer boundaries and their cleavage planes (Figure 5a to d).It appears that biotite acts as redactant, precipitating the uranium. Chlorites, sericeitized plagioclase and highly fractured quartz grains also contain uranium

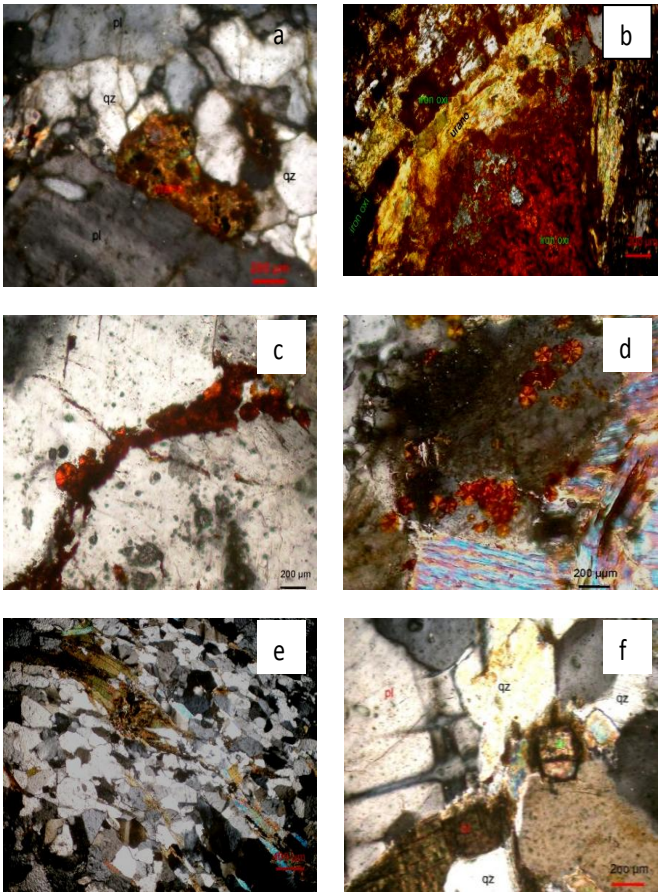

Figure 4. Photomicrographs showing: (a) Uranophane crystal (urano.) intersitial between quartz and plagioclase; (b) uranophane associating iron oxides (iron oxi.); (c) autonite occurs as flling fracuture in quartz; (d) autonite on the surface of crystals; (e) metamict zircon (zr).

mineralization (Figure 5e and f). Most of the rocks forming minerals are stained with iron oxides which occasionally adsorb uranium causing intense uranium mineralization (Figure 5g and h).

Radionuclides investigation

The radioelement measurements of the studied metamorphosed sandstone samples are shown in Table 1. Metasediments show wide variation in their U, Th, Ra (eU) and K% contents. They show variation of U from 3 to 24 ppm, with an average of 10 ppm and Th content between 2 and 47 ppm, with 14.57 ppm as an average. Ra (eU) vary between 2 and 18 ppm with an average of 8.07 ppm (Table 1).

When the data of the studied metasediments are compared with the averages of arenaceous and argillaceous sediments (Table 1) reported by IAEA (1979) and Boyle (1982), it is clear that Wadi Sikait samples have higher contents of uranium and thorium than the arenaceous sediments and also the average of greywacke reported by Killeen (1979). Average of uranium contents are higher than argillaceous sediments while average of thorium values fall within the range of argillaceous sediments. Th/U ratio average (1.59 ppm) is lower than average of arenaceous and argillaceous sediments. It is worth to mention that the relatively high values of U and Th in the studied metasediments are mainly related to the presence of radioactive accessory minerals such as metamict zircon, monazite, xenotime, allanite, uranophane and autonite observed in their thin sections.

The U-contents and Th/U ratios in sedimentary rocks are generally used to deduce the conditions under which the highly anomalous mineralized or uraniferous types were formed (Adams and Weaver, 1958). However, three types of sediments are differentiated according to their Th/U ratios:

i) The first type includes sediments of Th/U ratio value ranging between 0.012 to 0.81. These sediments are developed under conditions where uranium was removed from its source and fixed in the sediments with continuous recharge.
ii) The second type of sediments has Th/U ratio value ranging between 1.47 to 1.49. They are characterized by their relatively high Th-content due to slightly more scavenging of U-content because of continuous leaching and recharging.
iii) The third type of sediments exhibits Th/U ratio value ranging between 1.49 and 5.47. These sediments reflect the poor weathering and rapid deposition of rock detritus. Therefore, the detrital radioactive minerals like xenotime, samarskite, thorite and

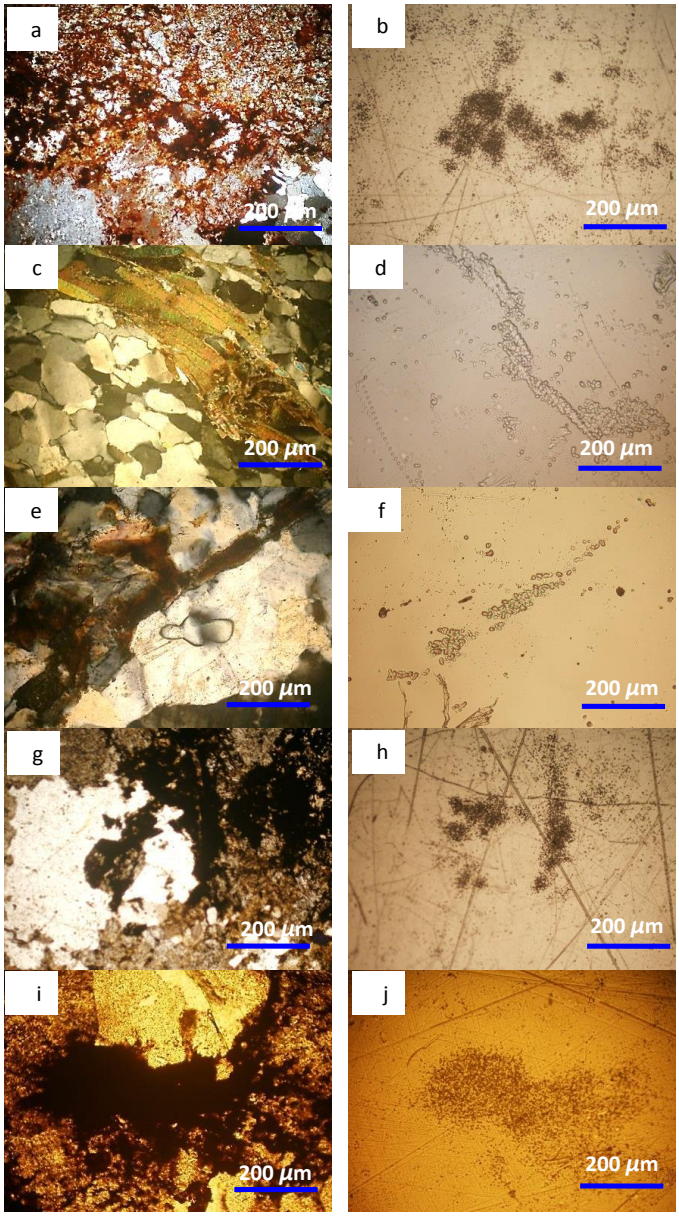

Figure 5. (a) Radioactive-mineralization along grain boundaries and in crystal lattice of allanite, zircon and monazite; (b) and its corresponding dense alpha track image showing radioactive minerals; (c, d, e and f) biotite and muscovitc grains are enriched in uranium mineralization along their outer boundaries and their cleavage planes and its corresponding dense alpha track image showing radioactive minerals; (g and h) chlorites, sericeitized plagioclase and highly fractured quartz grains also contain uranium mineralization; (i and j) iron oxides stained with uranium causing intense uranium mineralization and its corresponding dense alpha track image showing dense and disseminated radioactive minerals.

euxenite usually dominate them.

The obtained data indicates that the eTh/eU ratio values of the metamorphosed sandstone are low to medium values, ranging between 0.11 to 4.33, with 1.75 as an average (Table 1 and Figure 6). This means that they are related to more than one group, suggesting different conditions prevailing during uranium deposition. A high uranium content of the metamorphosed sandstone is attributed to presence of radioactive minerals like uranophane and autonite (Figure 4a and b) in addition to accessory minerals like allanite, zircon and monazite (Figure 5c to f).

Table 1. U, Th, Ra (eU) and K contents and some isotopic ratios.

Sample No.	Cup No.	Sample code	eU (ppm)	e Th (ppm)	Ra (eU) (ppm)	K%	Th/U	P-factor U/Ra	U_C	D-factor
1	45	N-S Sh 1-1 (1)	7	11	4	3.86	1.57	1.75	-	-
2	45	N-S Sh 1-1-(2)	4	9	5	3.35	2.25	0.8	-	-
3	42	N-S Sh1-1 (1)1	5	7	4	2.79	1.4	1.25	-	-
4	43	N-S Sh1-1 (1) 2	8.58	16.69	8.01	2.7	1.95	1.06	-	-
5	42	N-S Sh1-1 (2) 2	5	2	5	1.53	0.4	1	-	-
6	43	N-S Sh1-1 (3) 1	8	10	4	3.45	3.33	0.75	-	-
7	43	N-S Sh1-1 (3) 2	3	13	5	4.64	4.33	0.6	-	-
8	25	N-S Sh 1-6 1	29.38	90.84	56.22	5.67	3.09	0.52	35	1.19
9	45	N-S Sh 1-7 2	7	5	4	3.28	0.71	1.75	-	-
10	32	N-S Sh 2-1 1	10.85	20.04	8.48	3.63	1.85	1.28	-	-
11	44	N-S Sh 2-1 2	8.32	9.98	9.78	2.36	1.2	0.85	-	-
12	50	N-S Sh 3-1 (1)	10.51	20.13	9.97	3.71	1.92	1.05	-	-
13	50	N-S Sh 3-1 (2)	19.63	38.89	17.27	4.04	1.98	1.14	60	3.06
14	51	N-S Sh 3-2 (1)	3	2	0	0	1.33	1	-	-
15	51	N-S Sh 3-2 (2)	7.21	16.86	7.16	2.94	2.34	1.01	-	-
16	50	N-S Sh 3-3 (1)	20	45	12	0.36	2.25	1.09	40	2
17	53	N-S Sh 3-3 (2)	9.2	21.6	8.75	2.41	2.35	1.05	-	-
18	54	N-S Sh 2-3 B (1)	18.9	51.54	11.75	0.76	2.73	1.61	-	-
19	54	N-S Sh 2-3 B (2)	20	40.55	14.25	1.31	2.03	1.4	-	-
20	49	N-S Sh 4-1 (1)	6	15	7	2.78	1.96	2.4	-	-
21	59	N-S Sh 4-1 (2)	41.97	5.44	48.3	2.22	0.13	0.87	-	-
22	67	N-S Sh 5-1 a (1)	16	17	9	3.11	1.06	1.78	100	6.25
23	68	N-S Sh 5-1 a (2)	10	15	10	2.77	1.15	1.3	-	-
24	69	N-S Sh 5-2 (1)	17.14	29.91	15.23	5.4	1.75	1.13	50	-
25	69	N-S Sh 5-2 (2)	24.85	2.84	16.21	2.33	0.11	1.53	-	-
26	32	NNE-SSW Sh 2-1 2	5	21	8	4.16	4.2	0.63	-	-
27	35	NNE-SSW Sh 2-2 1	7	2	5	5.11	0.29	1.4	-	-
28	35	NNE-SSW Sh 2-2 2	7	2	5	4.52	0.29	1.4	-	-
29	33	NNE-SSW Sh 2-3 1	17	16	16	0.35	0.94	1.06	20	-
30	33	NNE-SSW Sh 2-3 2	8.41	12.6	9.02	3.1	1.5	0.93	-	-
31	63	NNE-SSW End of zone2 (1) at 63	15	22	7	2.03	1.47	2.14	-	-
32	63	NNE-SSW End of zone2 (2) at 63	7	13	6	3.93	1.86	1.17	-	-
33	37	*NW-SE* Sh 3-1 1	15	19	8	4.26	1.27	1.88	-	-
34	36	NW-SE Sh 3-1 2	9	19	9	4.46	2.11	1	-	-
35	38	NW-SE Sh 3-2 1	12	21	8	4.14	1.75	1.5	-	-

Table 1. Contd.

36	38	NW-SE Sh 3-2 2	10	18	9	4.14	1.8	1.11	-	-
37	39	NW-SE Sh 3-2 R 1	10	17	7	4.09	1.7	1.43	-	-
38	39	NW-SE Sh 3-2 R 2	12	16	7	4.93	1.33	1.71	-	-
39	40	NW-SE Sh 3-3 1	9	22	11	3.2	2.44	0.82	-	-
40	40	NW-SE Sh 3-3 2	16	23	10	3.39	1.44	1.6	-	-
Average			12	19	10.64	3.18	1.75	1.24	50.83	2.77
Minimum			3	2	0	0	0.11	0.52	20	1.18
Maximum			41.97	90.84	56.22	5.67	4.33	2.4	100	6.25
Arenaceous sediments (IAEA, 1979; Boyl, 1982)			1	3	-	1.4	3	-	-	-
Argillaceous sediments (IAEA, 1979; Boyl, 1982)			4	16	-	2.7	4	-	-	-
Average of greywacke (Killen, 1979)			1.5	5	-	-	-	-	-	-

Other U-bearing minerals are also recorded as biotite, muscovite, iron oxides and clays (Figure 5i and j).

Radioactive equilibrium

Both U and Ra are mobile from a chemical point of view. At this step we just can observe that disequilibrium exists, but we do not know if it is due to a U enrichment or a Ra impoverishment. According to Reeves and Brooks (1978), uranium (U^{238} series) attains the equilibrium state in nearly 1.5 M.a. Cathelineau and Holliger (1987) stated that uranium mineralization is affected by different processes. Leaching, mobility and redistribution of uranium are affected by hydrothermal solutions and/or supergene fluids which cause disequilibrium in the radioactive decay series in the U-bearing rocks. The radioactive equilibrium of the studied metasediment can be determined by the calculation of equilibrium factor (P) which is the ratio of radiometric uranium contents (eU) to the radium content Ra(eU); P_{factor} = eU/Ra(eU) (Hussein, 1978; El-Galy, 1998; Surour et al., 2001; Raslan and El-Feky, 2012; Nadaa and Aly, 2014).

The average of P-factor of the studied metasediment is 1.24 (Table 1), indicating disequilibrium in U-decay is due to addition of uranium to these rocks. The second method for the study of equilibrium is carried out by using the data of chemically analyzed uranium (U_c) and radiometrically determined uranium (U_r). Ratio between chemically and radiometrically measured uranium is known as the D-factor = Uc/U_r (Hansink, 1976). The use of D-factor in the determination of equilibrium state of the studied rocks reveals that nearly all the studied rocks have chemically analyzed uranium greater than the radiometrically determined uranium reflecting a disequilibrium state characterized by addition of uranium.

Evidences of recent uranium mineralization

Radiometric techniques (gamma-ray spectrometry, particle track analyses), in addition to chemical analysis were employed to determine the abundance and distribution of U-series nuclides, the extent of secular equilibrium within the U decay series. Young deposits are of apparent economic interest in view of their common occurrence, amenability to *in situ* leaching and lack of radioactive components. The uranium tends to be loosely held in recent uranium deposits and as it is too recently deposited to have built up radioactive daughter products; concentrations are seldom detectable by scintillometer. Though there was detection of surficial uranium mineralizations in the studied rocks by microscopic and α-track investigations and as a result of their young ages, the studied deposits have not yet reached radioactive secular equilibrium and therefore, yielded very little gamma activity (Table 1). Also, there is an apparent difference between radiometrically and chemically measured uranium (Table 1), suggesting recent U-deposition. The immobility of Th is supported by whole-rock Th contents which do not vary significantly with U content (Figure 6). Activity ratios (AR) of $^{230}Th/^{234}U$ in rocks, which range from 0.43 to 1.3, demonstrate recent U accumulation and leaching (Hassan et al., 2014), suggesting recent uranium mineralization.

Radon exhalation rates from the studied rocks were measured using ‘‘Sealed Can technique” and indicated the presence of subsurface and surface uranium anomaly which confirms the previous results (Hassan et al., 2014).

Conclusion

The metamorphosed sandstones occur in two locations in Wadi Sikait (Sikait-1 and Sikait-2). The main outcrops are ophiolitic mélange, metamorphosed sandstones, biotite granites and post-granite dykes (lamprophyres) and veins (fluorite and quartz). Radiometrically measured uranium contents reach up to 41.97 ppm while

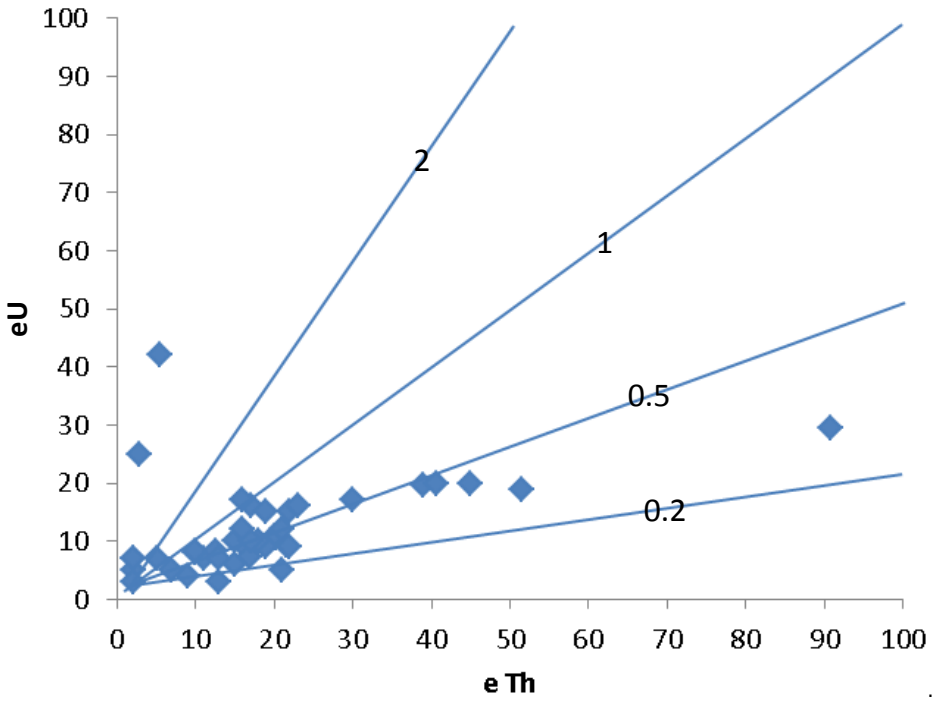

Figure 6. eU-eTh diagram of the studied metamorphosed sandstone.

chemically recorded measurements reach 100 ppm. High uranium contents may be attributed to the presence of uranophane, autonite, zircon, monazite, allanite, iron oxides and clay minerals.

Radiometric techniques and chemical analysis were employed to determine the abundance and distribution of U-series nuclides, the extent of secular equilibrium within the U decay series. Though in the detection of surficial uranium mineralizations in the studied rocks by microscopic and α-track investigations and as a result of their young ages, the studied deposits have not yet reached radioactive secular equilibrium and therefore, yield very little gamma activity. Also, there is an apparent difference between radiometrically and chemically measured uranium, suggesting recent U-deposition. The immobility of Th is supported by whole-rock Th contents which do not vary significantly with U content. Activity ratios (AR) of $^{230}Th/^{234}U$ in rocks, which range from 0.43 to 1.3 demonstrate recent U accumulation and leaching, suggesting recent uranium mineralization. Radon exhalation rates from the studied rocks were measured using "Sealed Can technique" and indicated the presence of subsurface and surface uranium anomaly which confirms the previous results.

Conflict of Interest

The author(s) have not declared any conflict of interests.

REFERENCES

Adams JAS, Weaver CE (1958). Thorium to uranium rations as indicator for sedimentary processes; An example of geochemical facies. Am. Assoc. Petrol. Geol. 42:397-430.

Assaf HS, Ibrahim ME, Zalata AA, El-Metwally A, Asaleh GM (2000). Polyphase folding in Nugrus- Sikeit area, south Eastern Desert, Egypt. JKAW: Earth Sci. 12:1-16.

Boyle RW (1982). Geochemical prospecting for thorium and uranium deposits. Elsevier Publ. Co., Amsterdam. P498.

Cathelineau M, Holliger P (1987). Polyphase metallogenesis of hydrothermal uranium veins from the southern amoricon massif, France. Proc. Int. Mtg Nancy. Pp.212-217.

El-Ramly MF, Greiling RO, Kroner A, Rashwan AA (1984). On the tectonic evolution of the Wadi Hafafit area and environs EDE, Bulletin Faculty Earth Science King Abdulaziz University 6:113-126.

El-Galy MM (1998). Geology, radioactivity, geochemistry and tectonic setting of selected granitic rocks, West Gulf of Aqaba, Sinai, Egypt, Ph.D Thesis, Tanta Univ.,Egypt. P.324.

Florou H, Kritidis P (1992). Gamma radiation measurements and dose rate in the coastal areas of a volcanic island, Aegean Sea, Greece.radiat. Port. Dosim. 45(1/4):277-279.

Greiling RO, Abdeen MM, Dardir AA, El Akhal H, El Ramly MF, Kamal El Din GM, Osman A F, Rashwan AA, Rice AHN, Sadek MF (1994). A structural synthesis of the Proterozoic Arabian–Nubian Shield in Egypt. Geol. Rundsch. 83:484-501.

Greiling RO, Kroner A, El-Ramly MF, Rashwan AA (1988). Structural relationships between the southern and the central parts of the Eastern Desert of Egypt: details of a fold and thrust belt. In: El-Gaby S, Greiling RO {Eds.). The Pan-African Belt of NE Africa and the Adjacent Areas-Tectonic Evolution and Economic Aspects of a Late Proterozoic Orogen. Frieder Vieweg and Sohn, Braunschweig/Wiesbaden, Germany, Pp.121-145.

Hansink JD (1976). Equilibrium analysis of sandstone rollfront uranium deposits. Proceeding of International Symposium on Exploration of uranium ore deposits. IAEA, Vienna. Pp.683-693.

Harraz HZ, EL-Sharkawy MF (2001). Origin of tourmaline in the

metamorphosed Sikait pelitic belt, south Eastern Desert. Egypt J. Afr. Earth Sci. 33(2):391-416.
Hashad AH, El Reedy MWM (1979) Geochronology of the anorogenic alkalic rocks, South Eastern Desert. Egypt J. Ann. Geol. Surv. Egypt. 9:81-101.
Hassan MA, Hashad AH (1990). Precambrian of Egypt. In: Said R. (ed.). The geology of Egypt, Balkema, Rotterdam, Pp.201-245.
Hassan SF, Abu Elatta SA, El-Farrash AH, El-Feky MG, Refaat M (2014). U-series radionuclides disequilibria as indication of recent U-mobilization in mineralized Low grade metamorphosed sandstone-type uranium deposit, Wadi Sikait, South Eastern Desert, Egypt, in press.
Hegazy HM (1984). Geology of Wadi El Gemal area, Eastern Desert, Egypt. Ph. D. Thesis, Assiut Univ., Egypt. P. 271.
Hussein HA (1978). Lecture course in nuclear geology. P. 101.
IAEA (1979). International Atomic Energy Agency. “Gamma-Ray Survey in Uranium Exploration”. IAEA Technical Report Series, No. 186, Vienna, Austria, P.90.
Ibrahim ME, Abdel-Wahed AA, Oraby F, Abu El-Hassan El Galy MM, Watanabe K (2007). factors controlling mineralization in lamprophyre dyke, Abu Rushied area, Eastern Desert, Egypt. 5 th International Conf. on the geology of Africa Assiut – Egypt. 1:79-92.
Ibrahim ME, Amer TE, Saleh GM (1999). New occurance of some nuclear materials and gold mineralization at Wadi Sikait area , south Eastern Deser, Egypt .First seminar on Nuclear Raw Materials and their technology,Cairo,Egypt. Pp.271-284.
Ibrahim ME, Saleh GM, Ibrahim WS (2010). Low grade metamorphosed sandstone-type uranium deposit, Wadi Sikait, South Eastern Desert. Egypt. J. Geol. Min. Res. 2(6):129-141.
Killeen PG (1979). Gamma ray spectrometric methods in uranium exploration—application and interpretation; *in* Geophysics and Geochemistry in the Search for Metallic Ores; Hood, P.J., ed., Geol. Surv. Can. Econ. Geol. Report 31:163-229.
Matoline M (1991). A report to the government of the Arab Republic of Egypt. “Construction and use of spectrometric calibration pads", Egypt. Laboratory gamma-ray spectrometry.
Mohamed FH, Hassanen MA (1997). Geochemistry and petrogenesis of Sikait leucogranite, Egypt: an example of S-type granite in a metapelitic sequence. J. Geol. Rundsch. 86:81-92.
Nadaa A, Aly HAS (2014). The Effect of Uranium Migration on Radionuclide Distributions for Soil Samples at the El-Gor Area, Sinai, Egypt. Appl. Radiat. Isotopes. 84:79-86.
Omar SA (1995). Geology and geochemical features of the radioactive occurrences of Um-Anab granitic masses, Eastern Desert, Egypt, M.Sc. Thesis, Cairo University. P.195.
Raslan MF, El-Fekyy MG (2012). Radioactivity and mineralogy of the altered granites of the Wadi Ghadir shear zone, South Eastern Desert, Egypt. Chin. J. Geochem. 31(1):30-40.
Reeves RD, Brooks RR (1978). Trace element analyses of geological materials. John Wiley & sons Inc., New York, P.421.
Saleh GM (1998). The potentiality of uranium occurrences in Wadi-Nugrus area, South Eastern Desert: Unpubl. Ph.D. thesis, Faculty of Science, Mansoura University P.171.
Saleh GM Abdallah SA, Abbas AA, Dawood NA, Rashed MA (2012). Uranium mineralizations of Wadi Sikait mylonites, Southeastern Desert. Egypt J. Geol. Min. Res. 3(5):86-104.
Stern RJ, Hedge CE (1985). Geochronologic and isotopic constraints of Late Preeambrian crustal evolution in the Eastern Desert of Egypt. Am. J. Sci. 285:97-127.
Surour AA, El-Bayoumi RM, Attawiya MY, El-Feky MG (2001). Geochemistry of wall rock alterations and radioactive mineralization in the vicinity of Hangaliya auriferous shear zone, Eastern Desert, Egypt. Egypt. J. Geol. 45(1):187-212.
UNSCEAR (1993). Sources and effects of ionising radiation. Report to general assembly, with scientific annexes, United Nations, New York.

Journal of Geology and Mining Research

volume 6 Number 2 March, 2014

ISSN 2006-9782

Related Journals Published by Academic Journals

- *Journal of Geochemistry Research*
- *International Journal of Geophysics and Seismology*
- *International Journal of Physics Research*
- *International Journal of the Physical Sciences*
- *African Journal of Pure and Applied Chemistry*

academicJournals